Materials Characterization 203 (2023) 113105

Contents lists available at ScienceDirect

Materials Characterization

journal homepage: www.elsevier.com/locate/matchar

Evaluation of synthesis time in the growth of vertical-aligned MWCNTs by spray pyrolysis

A. Garzon-Roman [a,b], A. Ferreiro [c], C. Zúñiga-Islas [a], M.E. Rabanal [c,*]

[a] Instituto Nacional de Astrofísica Óptica y Electrónica, Calle Luis Enrique Erro, Santa Maria Tonantzintla Puebla, C.P. 72840, Mexico
[b] Institute of Physics, Benemérita Universidad Autónoma de Puebla, PO Box J-48, 72570 Puebla, Mexico
[c] Materials Science and Engineering Department and IAAB, Universidad Carlos III de Madrid, Avda de la Universidad, 30, 28911 Leganes, Spain

ARTICLE INFO

Keywords:
Vertically-aligned carbon nanotubes
Spray pyrolysis
Porous silicon
Well-graphitization

ABSTRACT

Multi-Wall Carbon Nanotubes (MWCNTs) were analyzed on crystalline silicon substrates (type P) under optimal temperature conditions, using different synthesis times (2, 3, 4, 5, 10, 20, 30, 60, 120, and 180 min) in order to examine the effect on the structural quality and length of the CNTs produced by ultrasonic spray pyrolysis, using pure toluene and ferrocene as precursor solutions under argon flow. Structural, optical, and morphological differences of the MWCNTs grown were analyzed. Raman spectroscopy evidenced the MWCNTs' high quality, noted by the I_D/I_G (from 0.41 to 0.68) and I_{2D}/I_G intensity ratios around 0.75. Morphological differences of the MWCNTs grow evaluated by Field Emission Scanning Electron Microscopy (FE-SEM); the micrographs examined the thickness of CNTs' layers. High-Resolution Transmission Electron Microscopy (HRTEM) technique was used to determine the diameters of CNTs, which were found from 15 to 140 nm. X-Ray Diffraction (XRD) showed two characteristic peaks around 26° and 44°, which corroborated that the MWCNTs were well-graphitized. The influence of the time in these CNTs demonstrated that the final length of these nanotubes could easily reach micrometers. The alienation was better as time increased, and the graphitization extent is good in most cases compared to other more expensive synthesis methods.

1. Introduction

Carbon is an element that can be hybridized in sp., sp^2, or sp^3 forms. In recent decades, new crystalline forms such as graphene, fullerenes, and carbon nanotubes have attracted attention. The CNTs, representing an allotropic form of carbon, have been studied extensively since they were discovered in 1991 [1]. Besides, carbon nanotubes come in two major types: single-wall and multi-wall. Both structures have been applied to different branches of science and engineering. In electronics fields, it is reported the development of different devices such as chemical sensors [2], photovoltaic devices [3], memory devices [4], field effect transistors [5], printed electronics, supercapacitors, ultralight composites [6–8], owing to the different CNT properties such as mechanical, electric, thermal and chemical. Moreover, the combination of these composites can help to improve the properties of the materials, and the nanotubes are potential candidates to be employed in the formation of composites. For example, Ali et al. [9] have revised how carbon nanotubes have been employed to create composites that can improve the required characteristic for a specific application as nanoparticle integration into an epoxy matrix and its fiber-reinforced composites [10]. This property is one of the main studies in the last decade, and therefore, composites fabrication could be applied in electronics, engineering plastics, energy storage, and the energy harvesting industry. These carbon structures are built using different carbon-based precursors and metallic catalyzers, and such structures are obtained through several methods which allow CNTs synthesis, such as electrolysis, hydrothermal method, ball milling, laser ablation, arc discharge, chemical vapor deposition (CVD) [9]. With these methods, we find conventional DC or AC arc discharge [11] or a method modified by applying a magnetic field [12], but the principle is the same, and it consists of applying a potential between two graphite rod electrodes until evaporating one of the carbon rods [11,12]. With this method, it is possible to obtain high-quality CNTs, though the main disadvantage is the high temperature needed for synthesis, besides the fact that an additional purification process is required. Another suitable method is laser ablation, which consists in the sintering of a graphite target

* Corresponding author at: Materials Science and Engineering Department and IAAB, Universidad Carlos III de Madrid, Avda de la Universidad, 30, 28911 Leganes, Spain.
E-mail address: eugenia@ing.uc3m.es (M.E. Rabanal).

https://doi.org/10.1016/j.matchar.2023.113105
Received 4 April 2023; Received in revised form 7 June 2023; Accepted 17 June 2023
Available online 20 June 2023

containing cobalt or nickel, even a mixture of both [13]. However, production is limited to the lab scale, and final purification processes are also necessary. Chemical vapor deposition (CVD) and its modifications [14–18] are considered one of the best approaches for large-scale production, according to Tsung et al. [19]. This method uses several carbon sources for growth, such as acetylene, ammonia, carbon monoxide, or ethylene. The CNTs are grown on different substrates or metal films that work as catalysts. The substrates or metal films used are nickel, cobalt, molybdenum, iron, etc. This method, which works at lower temperatures (<800 °C), is manageable and cheap with high purity, large-scale production, and suitable to grow aligned CNTs.

However, with the CVD method, the CNTs could include some defects, and they usually synthesize MWCNTs, and much more, there is a constant risk with the atmosphere used in the furnace. Nowadays, CVD is still being used for the production of CNTs, but this method can be simplified and used for large-scale production, and this thanks to injecting metallocene-hydrocarbon solutions into a heated quartz reactor, catalyst particles and carbon nanotubes can be formed simultaneously [20].

On the other hand, spray pyrolysis (SP) has widely been used to obtain transparent conductive oxide films (TCOs) [21] and thin films of metals [22]. Recently, this method has gained attention and importance because carbon structures (graphene or carbon nanotubes, for instance) have been obtained on a commercial scale [23–28]. Moreover, with SP, the CNTs have been obtained with different lengths, certain alienation, and continuous growth [23–28]. This technique is like CVD, but there is no risk of using dangerous atmospheres. Kamalakaran et al. [26] have explained the synthesis mechanisms of these CNTs. Previously, metal cluster particles were deposited on the substrate surface, acting as carbon traps, leading to CNTs growth. However, an important characteristic is the adhesion between the substrate surface and the metal catalyst particle since the metal particle can stay in the base or tip or even along the nanotube during the growth, as claimed by Kamalakaran et al. [26].

In this work, we have studied the chemical, morphological, and structural characteristics of the synthesis of MWCNTs by SP concerning deposit time. Also, we have shown that this technique is straightforward and can be applied to grow MWCNTs with high quality and long lengths aligned >300 μm.

2. Material and methods

The CNTs were prepared by the experimental set-up shown in Fig. 1 (similar to the reported set-up in the literature [23–25], but with some modifications). The set-up consisted of ultrasonic equipment operating at 800 KHz to obtain a mist of tiny drops of hydrocarbon/catalyst, an electric furnace equipped with a quartz tube (8.8 cm internal diameter), two collector traps, and silicon substrates placed in the quartz tube. A constant amount of ferrocene (35 g) was dissolved in pure toluene volume (1000 ml). The quartz tube was first flushed with Ar to eliminate any oxygen present and also was used as a carrier gas to generate the ferrocene/toluene mist in the nebulizer. The quartz tube was heated by a cylindrical furnace at 780 °C. After 45 min, when the furnace had just reached the steady state temperature, the ultrasonic cavitation process began, and a constant Ar flow at a rate of 2 ml/min during all the experiments was fixed. After the time variation, the precursor supply was terminated, and the reaction chamber was cooled gradually, keeping a constant Ar flow until room temperature (RT). Times of 2, 3, 4, 5, 10, 20, 30, 60, 120, and 180 min were evaluated (samples labeled as M2, M3, M4, M5, M10, M20, M30, M60, M120, and M180, respectively) on the structural, morphological and functional properties of MWCNTs obtained.

Different characterization techniques to evaluate the influence of synthesis time were used. Raman spectroscopy was performed by Renishaw Invia Raman spectrometer. At ambient conditions, an argon Ar^+ laser of 532 nm and 30 mW as an excitation source operated at 5% power was applied to excite the sample through a 50× objective lens. In addition, the samples were analyzed by HR-TEM, JEOL JEM-3000F, operated at 300 kV to corroborate the formation of nanotubes. All samples were prepared by scratching off some of the black layers from the silicon substrate, dispersing and sonicating in pure acetone for 60 min, and depositing a drop of the solution in a carbon-coated copper TEM grid, and then examined by HRTEM. FE-SEM was employed to characterize the samples' morphologies, size, and structure using a FEI TENEO Scanning Electron Microscope in cross-section. The XRD was obtained by Panalytical X'Pert 30 operated at 40 Kv using a CuKa radiation (1.54°) from 20 to 60° in 2Θ.

3. Results and discussion

By Raman spectroscopy, the MWCNTs' growth with time was evaluated. Fig. 2A and B show the Raman spectra of the MWCNTs deposited on silicon substrates at different synthesis times. As can be seen from the graphs, the three main characteristic bands, the D-band, G-band, and 2D-band, are evident in all samples. The D-band peak at 1343 cm^{-1} could be related to defects and lattice disorders in the sp^2-hybridized carbon and/or amorphous carbon, as seen in [28–32]. Another possible origin proposed by Rao et al. [33] is that the D band intensity may also be due to polarization effects within aligned CNTs' bundles and not necessarily arise only from disorder. The G-band around 1570 cm^{-1}corresponds to the tangential stretching mode of carbon atoms in the graphene wall of MWCNT [34]. However, Zou et al. argue that the G-band is due to a number of sp^2 hybrid carbon atoms [28]. Hence, it is not

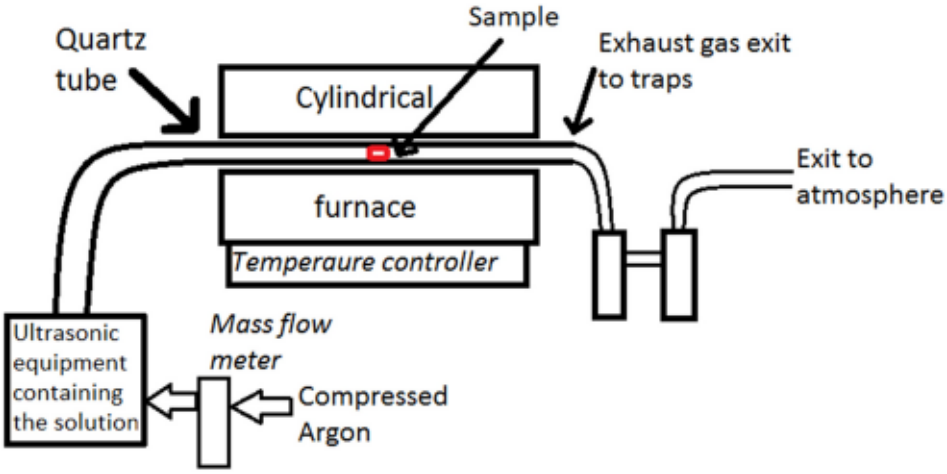

Fig. 1. Schematic illustration of the experimental set-up used to obtain MWCNTs.

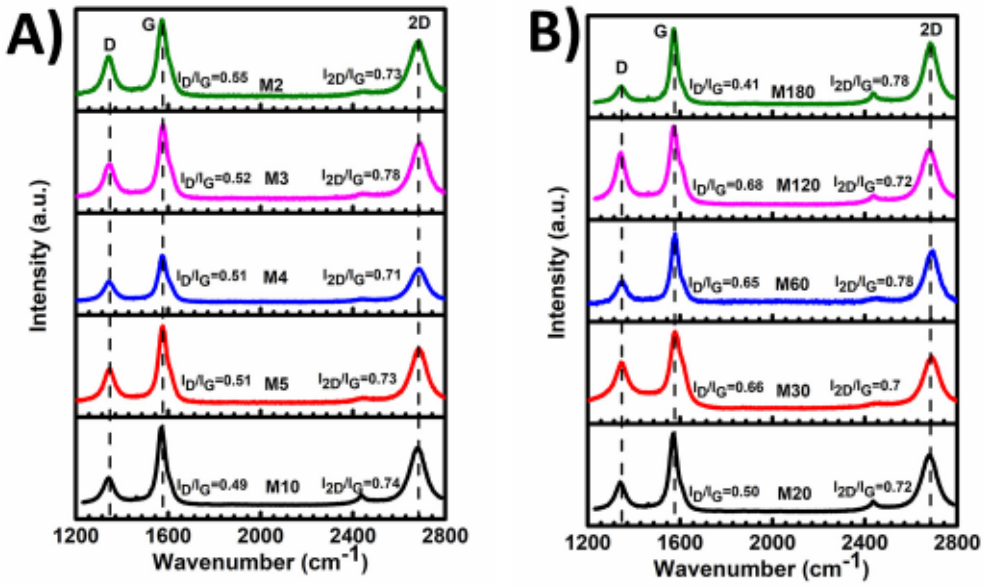

Fig. 2. Raman spectra of CNTs grown on silicon substrates A) for 2, 3, 4, 5 and 10 min B) 20, 30, 60, 120, and 180 min.

clear what the origin of this band is, which is also a key research topic. The 2D-band peak at 2679 cm^{-1} is ascribed to the highest optical branch phonons near the K point at the Brillouin zone boundary [28]. The ratio of the integrated intensity of the D band to that of the G band (I_D/I_G) is a good indicator of graphitization in the samples [28,35]. Zou et al. pointed out that the relative intensity ratio of 2D and G can be used to estimate the layers' number for graphene [28]. The integrity intensity ratios $I_{2D}/I_G > 2$, $I_{2D}/I_G > 1$–2, and $I_{2D}/I_G < 1$ correspond to single-layered, double-layered, and multilayer graphene, respectively, according to the literature [28,36,37]. Therefore, these ratios could be applied to estimate the layers' number of CNTs grown in our experiments. Raman spectra and the ratios calculated are shown in Fig. 2, and Table 1, respectively.

The intensity I_D/I_G ratio is similar to the MWCNTs grown at short synthesis times ($t < 20$ min) with values lower than 0.6. In the case of higher synthesis times ($t > 30$ min), the graphitization value is higher than 0.6, except for the sample at $t = 180$ min, which presents the lowest graphitization value. The average of graphitization for all samples is 0.54, which indicates that the quality in these samples is good and the amount of amorphous carbon could be considered low. In fact, Tan et al. [38] reported similar values $I_D/I_G = 0.43$ for CNTs prepared by the arc discharge technique. This shows that ultrasonic spray pyrolysis is a suitable, easy, and cheap method for CNTs synthesis with a high graphitization extent. Nevertheless, the relation I_{2D}/I_G ended up as <1, which suggests that the number of walls could be high. Remarkably, all samples present the I_{2D}/I_G ratio around 0.73 ± 0.1 implying a similar number of layers in the CNTs.

On the other hand, it could have been possible to observe a weak D′-band or shoulder around 1615 cm^{-1} in all samples, as is reported in [39–41]. This is attributed to disorder induced in the carbon due to particle size distribution or lattice distortion [42]. This shoulder is more evident in the samples M120, M60, and M30, corresponding to the samples with the worse graphitization extent above 0.6. Therefore, this shoulder could be another option for knowing the quality of the samples.

If we divide the samples into two groups, we can find a correlation between the intensity ratios of D/G and growth time. For example, the synthesized samples from 2 to 10 min have reduced the ratio, increasing the graphitization extent. Therefore, as the synthesis time increases, the ratio decreases. Afre et al. [23] argue that the decrease in the ratio is attributed to a large amount of amorphous carbon present in the grown films. However, the decrease is attributed to the increase of graphitization in the samples; it means the D band is smaller than the G band due to small ratios between these two bands [28,35,38,and]. While the ratios of intensities are small or the D-band is small, there will be a high extent of graphitization.

For the second group with the synthesis times, 20, 30, 60, 120, and 180 min, the ratio increases (except for the M180 sample), indicating that the graphitization extent decreases, given the M120 sample's worse graphitization extent. However, the M180 sample showed the best graphitization extent, which could be due to the perfect formation and alignment of CNTs in comparison with other samples. This will be discussed later.

Finally, the ratio of 2D/G did not present a relation like D/G, but the ratios found in the samples demonstrated that the CNTs are formed by multi-walls. Even that small difference between the ratios can show the difference in the diameter of the CNT according to the number of graphene sheets wrapped. All the samples generally had a 2D/G ratio < 0.8, predicting the CNTs formation with multilayers of graphene.

SEM micrographs of vertical cross-sections of CNTs grown on the silicon substrate are pointed out in Fig. 3A to 3J. In the images, it is possible to observe vertical columns though some are more vertical than others. These arrays consist of countless nanotubes self-organized into a fiber-like structure. As can be seen in Fig. 3C to 3J, a fiber-like structure is evident, contrary to the CNTs arrangement exhibited in Fig. 3A, and B,

Table 1
Raman spectroscopy of CNTs: G, D, and 2D peak intensity ratio.

Sample	M180	M120	M60	M30	M20	M10	M5	M4	M3	M2
Time cavitation process in min	180	120	60	30	20	10	5	4	3	2
Ratio I_D/I_G	0.41	0.68	0.65	0.65	0.50	0.49	0.51	0.51	0.52	0.55
Ratio I_{2D}/I_G	0.78	0.72	0.78	0.7	0.72	0.74	0.73	0.71	0.78	0.73

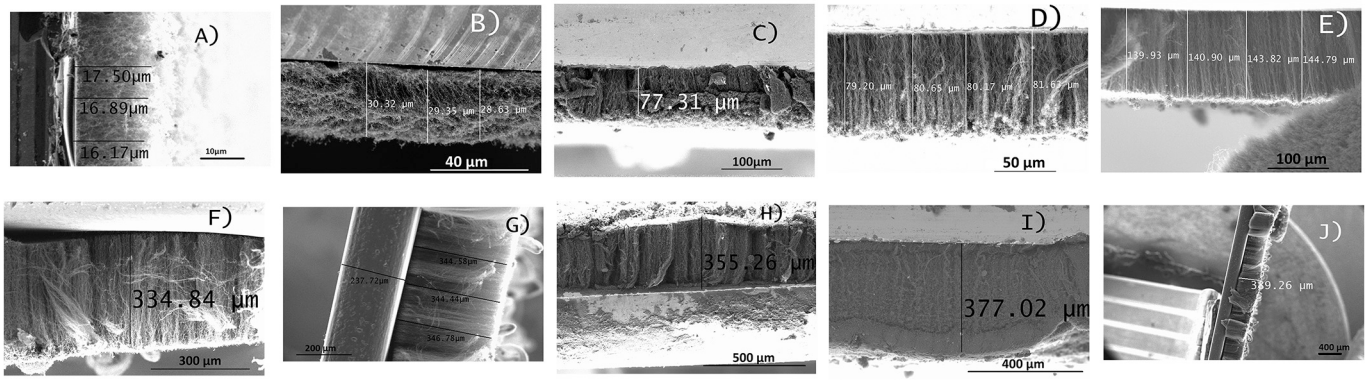

Fig. 3. FESEM cross-section of CNTs grew on silicon substrates varying the growth times: (A) 2 min, (B) 3 min, (C) 4 min, (D) 5 min, (E) 10 min, (F) 20 min, (G) 30 min, (H) 60 min, (I) 120 min, and (J) 180 min.

which show structural arrangements not well-defined. It is interesting to note this disorder since it can lead to a presumable relation between the structural disorder and the growth time parameter. We emphasize that this disorder is more evident in Fig. 3B, even though some nanotubes neither grew in a well-defined vertical way nor took a curved form (Fig. 3A and B).

According to the SEM pictures, we tried to get the CNTs' layer thickness measured from the substrate base to the top tip of CNTs; in some cases, it was not easy due to the not well-defined arrangement found (Fig. 3B). However, some measurements vary approximately from 17.5 3.1 m up to 389.5 10.3 m. In Table 2, the length of CNTs is shown. Such variations originated due to the different growth times used. On the other hand, the use of silicon substrates as supports results advantageously since on the surface of silicon, there is always a native SiO_2 layer, which plays the role of strong support, where the catalytic activity together with the carbon atoms helps nanotubes to grow longer [43]. Starting from Fig. 3C up to 3 J, a very flat surface of the film is shown, which allows us to observe that the length of aligned nanotubes varies. Moreover, something to note is that from Fig. 3F until 3 J, the lengths of CNTs start to be the same, indicating a saturation in the carbon nanotube length. Another point of interest is that some films showed different deformations (crushed structure or non-adherence on the substrate, for instance) generated perhaps during the deposit process or while the films were manipulated in the measurement stage.

The ordered packing of CNTs from the effect of the Van der Waals interaction results in the CNTs' alignment formation. In the literature, several works report the growth of CNTs on silicon substrates using different methods, but few of them speak of the effect of varying time from short to long times in the growth process.

Afre et al. observed that the growth process of CNTs takes place preferentially on the bottom side of the substrate rather than on the top side [23]. However, an interesting feature can be observed in Fig. 3H where the growth process does not occur preferentially as Afre et al. observed [23]. The CNTs grew on different sides of the substrate, including on the edge, creating a problem since we had to scratch its edges to measure and identify the silicon substrate.

The slow flow of the solution's vapor is responsible for this growth, as only one Fe particle is necessary to start the growth, which facilitates this effect on the silicon substrates. On the other hand, something interesting is the CNTs' growth density, as this density increases as time increases due to the density of catalytic Fe particles deposited on the silicon substrate. Looking at Fig. 3D) through 3 J), the CNTs density is higher than in other samples. Table 2 shows the CNTs layer thickness estimated.

We believe that irregularities found in Fig. 3A and B could be due to the mechanism of CNTs growth from solution drops in the mist fed to the reaction chamber. After the typical reaction of pyrolysis on catalyst/hydrocarbon mixture drops, particles of Fe and amorphous graphite are formed, and after that, these nanoparticles reach the surface of the silicon or incorporate into CNTs which are already growing. Even the irregular CNT walls become aligned during the synthesis due to the temperature. Hence, with the short times, the sufficient amount of particles to saturate the substrate surface is not reached, and the substrate does not stay the necessary time at the optimal temperature, resulting in the CNTs not well-aligned like the one shown by the samples with longer times. In other words, the thickness and the alignment of the CNTs depend strongly on the synthesis time, which means there is an alignment for t 4 min while the growth temperature is maintained.

According to Table 2, from 20 min to 180 min, the length almost stays constant. This effect could be due to the formation of an additional layer of carbon on the tip-growth (Fig. 3H and I), producing a discontinuity in the growth and avoiding the increase in the length like that shown in Fig. 3F, G, H and I. Another alternative to explain this behavior is the high density in the sample, as the tips of CNTs start to agglomerate and take a fiber-like structure, and the tips are closed or bent, preventing new iron seeds for continuous growth. On the other hand, different growth mechanisms exist where nanotubes are formed, and more than one mechanism might be functional during this stage. Chen and Zhang [44] proposed a mechanism of three steps. First, a precursor is formed on the surface of the metal particle. Second, the CNT is rapidly formed by the metastable carbide particle. Lastly, there is slow and continuous graphitization.

Another growth mechanism for CNTs was postulated by Sinnot et al. [45]; they infer that metal particles are supported on the substrate or are introduced as floating particles. If the particles are spherical or pear shape, the deposition of these particles will take place on only half of the surface. Then the carbon diffuses along the concentration gradient and precipitates onto the opposite half, around and below the bisecting diameter. However, it does not precipitate from the apex of the hemisphere, which accounts for the hollow core that is characteristic of these filaments [45]. For supported metals, filaments can form either by 'extrusion or root-growth in which the fiber grows upwards from metal

Table 2
Thickness of CTNs layer with cavitation times evaluated.

Time cavitation process (min)	180	120	60	30	20	10	5	4	3	2
Labeled sample	M180	M120	M60	M30	M20	M10	M5	M4	M3	M2
CNTs layer thickness (m)	389 23	377 20	355 15	344 18	334 10	142 5	80 8	78 6	29 3	16 1

particles that remain attached to the substrate, or the particles detach and move at the head of the growing fibers, labeled 'tip-growth [45]. According to Fig. 4, it is observed that the majority of metal particles were found on the substrate (that indicates a good adherence between the substrate and the particles, and the zoom-in image can appreciate the iron particles deposited), and some particles were found along the CNTs. Therefore, the metal particles work as a base for the growth of CNTs, and the extrusion or root-growth model fits this synthesis process. The inset in Fig. 4 shows the particle size and some CNTs grown. R. Andrews et al. [46] have suggested that the catalyst particle size determines the size of the CNT. In the TEM images, this hypothesis will be assessed.

Fig. 5 shows the TEM images of CNTs synthesized at 780 C with Ferrocene/Toluene. As can be seen, it consists of a fiber-like structure containing metal nanoparticles and not any amorphous carbon. The particles are distributed mainly on the top of the CNTs, but sometimes it is possible to find these metal particles inside of the CNTs. These nanoparticles sometimes show a diameter bigger or smaller than the nanotube (Fig. 5A, B); hence the hypothesis by Andrews et al. [46] could not be acceptable to all. This is due to the samples are composed of fibers. Noticeable iron particles can be seen inside the fibers, which are made up of many carbon nanotubes. The iron particles can be removed by liquid-phase oxidation using HNO_3 or H_2SO_4:HNO_3; However, the problem is the reaction with the CNTs themselves, which can cut and even open the walls and insert functional groups. Also, HCl as non-oxidative acid, has been used with good results in the purification of CNTs. However, these nanoparticles can help for the formation of composites as fiber reinforced, which has been a feature very studied in the last decades, as we mentioned previously in the introduction [47].

On the other hand, in Fig. 5 it is possible to observe two formations of CNTs'. In Fig. 5B many CNTs are entangled and bending, which makes agglomerates of these nanotubes. These agglomerates can produce the effect observed in the Raman measurements as a high intensity in the spectra. Fig. 5C can be appreciated well-defined nanotubes without agglomerates nir fibers; Fig. 5D shows nanotubes with the biggest diameters around 70 nm; this corresponds to the sample with the longest synthesis time (180 min). In this last sample, fibers could not be identified as in other samples due to the high graphitization extent. Moreover, metal particles were found in the tip and inside of the nanotube. The diameter of the nanotubes increases as time increases, being able to be related to the metal particle size. The particle size rules the smallest nanotubes, but as time increases, the metal particles create agglomerate, and the diameter increases. The particles found inside nanotubes could be floating debris that were introduced during the synthesis process.

Fig. 6 shows the HRTEM images, and the inset images correspond to the diffraction patterns of a CNT or a metal particle. HRTEM images confirm that CNTs are formed by many graphene sheets following the parchment model, corroborating the 2D/G intensity ratio as the CNT formation by many graphene layers. It could be observed that these CNTs are inside each one, causing the increase in the diameter (Fig. 6B). The perfect alignment and parallelism among the graphene sheets are evident, which indicates a high graphitization extent of the samples.

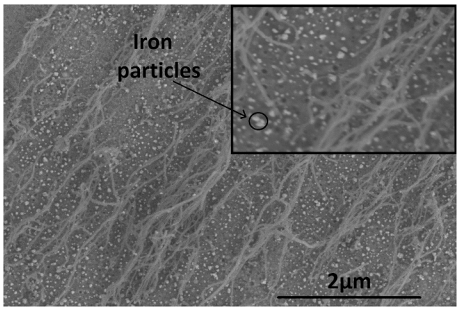

Fig. 4. Planar view of iron particles and aligned CNTs on the silicon substrate.

Moreover, Fig. 6C presents the metal particles covered by carbon. In general, the MWCNTs are closed structures, and for that reason, the metal particle is covered. However, as could see in the images of low-magnification, these particles can be present along the CNT or at the end of the nanotube. With most of the growth times, the particles are like spheres, but sometimes, a slight agglomeration among the particles exists and causes deformation. The smallest particles form bigger agglomerates, producing CNT with diameters above 20 nm of a like-fibers structure due to entanglement among these nanotubes. Moreover, as the 2D/G intensity ratio showed, the CNTs are composed of many layers of graphene; Fig. 6A can corroborate that at least there are 5 graphene layers for the thinnest nanotubes and 20 graphene layers for concentric nanotubes that form little fibers (Fig. 6B).

On the other hand, for the diffraction patterns, all samples present continuous rings and diffused halos. It is well-known that the continuous rings indicate a random orientation of neighboring crystallites, and diffused halos indicate an amorphous background, which could be due to the presence of amorphous carbon in the thin layer that covers the CNT.

XRD patterns of some samples of MWCNTs are shown in Fig. 7. Some patterns displayed an intense diffraction peak around 2 26 in orientation (002); also, a low intensity was shown in 44 with preferential orientation (100). In the literature, other peaks around 53 and 78 are reported [44]. However, these diffraction peaks could not be found in the samples. Besides, these results confirm that MWCNTs are well graphitized [48]. Therefore, this corroborated the high graphitization extent observed from Raman spectra and HRTEM images. Moreover, XRD showed a slight shoulder around 43 due to the metal particles, but the intensity of this peak was extremely low. Hence, this indicated that the amount of these metal particles was reduced compared with CNTs, as observed in the HRTEM, and thus, these metal particles preferred to stay attached and anchored on the silicon substrate. These results showed that a purification process is not necessary.

4. Conclusions

Carbon nanotubes were obtained successfully by ultrasonic spray pyrolysis using Ferrocene/Toluene precursor solution and at low-temperature (780 C) synthesis. CNTs were grown perpendicularly on silicon substrates; for some cases, these nanotubes were highly aligned, as the SEM images corroborate. Something important that could be noted is that for times above 20 min, the length of these arrays almost kept constant (~350 m). The Raman spectra show the three characteristic bands, and the ratios between D-band and G-band intensity revealed a high extent of graphitization, which is comparable with other more expensive methods. Additionally, the 2D-band and G-band ratios and HRTEM images have confirmed that the CNTs are formed by some graphene layers. The SEM images show a high alignment and a fiber-like structure and reveal the thick layer of the CNTs. SEM images exposed a better alignment from 5 min to 180 min samples than the 2, 3 and 4 min ones, but times 20 min except 180 min demonstrated the better graphitization extent according to the Raman measurements. Some closed variations indicate that the growth times do not affect the diameter of CNT very much.

Further, metal particles were observed at the end of the CNT and inside the CNT. The metal particle size adhered on the silicon substrate was around 30 nm (according to SEM images), but the TEM images showed that these particles can or cannot create agglomerations resulting in bigger or smaller particles inside the CNT. TEM images in high magnification revealed the multi-walls of the CNTs, their perfect alignment, and parallelism among them. Furthermore, it is possible to observe some graphene sheets forming the CNTs following the parchment model. The diffraction patterns obtained by TEM images showed rings demonstrating the crystallinity and diffused halos indicating amorphous background like amorphous carbon. The XRD diffractograms supported the good graphitization extent previously discussed

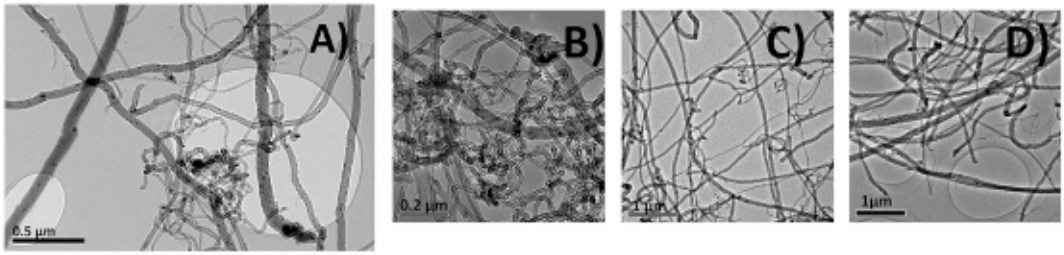

Fig. 5. TEM images of CNTs at low magnification at different times: (a) 4 min, (b) 10 min, (c) 20 min, (d) 180 min.

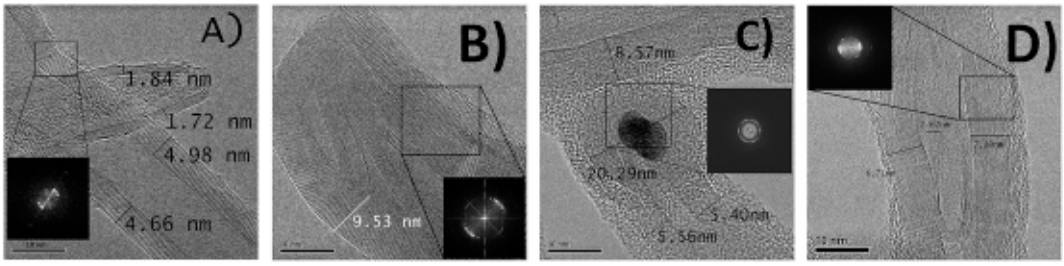

Fig. 6. TEM images of CNTs at high magnification at different times: (a) 4 min, (b) 10 min, (c) 20 min, (d) 180 min.

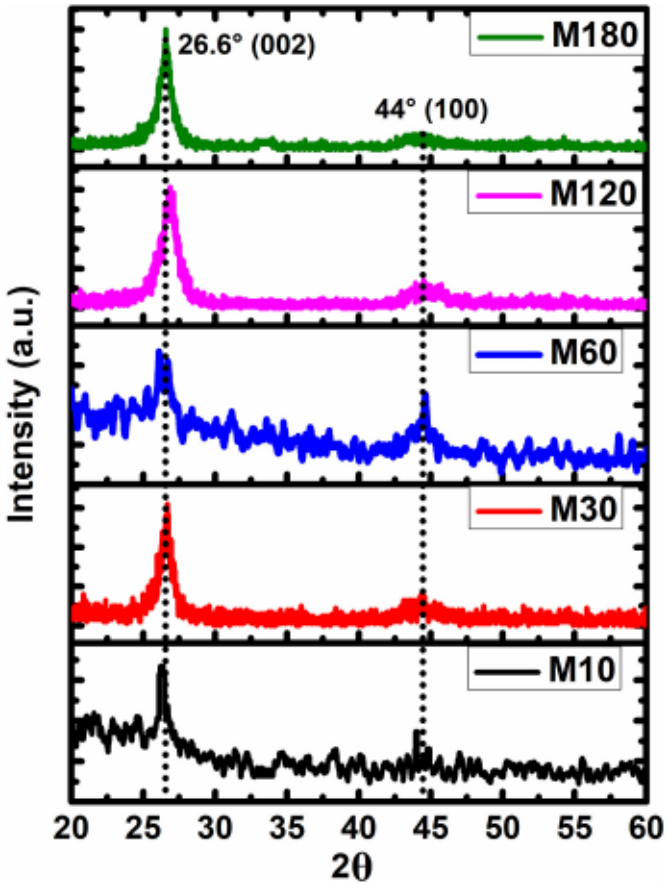

Fig. 7. XRD patterns of MWCNTs for different growth times 180 min, 120 min, 60 min, 30 min, and 10 min.

according to Raman spectra and TEM images. Longer growth times demonstrated that reaching lengths around the micrometer scale is possible, with a good alienation and even a high graphitization extent.

In conclusion, this work shows the great opportunities of ultrasonic spray pyrolysis for the CNTs industrial production since it is easy, cheap, and generates high-quality CNTs.

Authors' contribution

A. G. Roman and M. E. Rabanal collaborated in order to propose the experiments, growth the carbon nanotubes, carry out the measurements and write the investigation. A. Ferreiro and C. Zúñiga-Islas reviewed and made the necessary corrections in this investigation.

Declaration of Competing Interest

The authors declare that they do not present any conflict of interest in this research.

Data availability

The raw/processed data required to reproduce these findings cannot be shared at this time as the data also forms part of an ongoing study.

Acknowledgments

We thank Technician Adrian Gómez Herrero, Technician Cristina Moral Gil and Hugo Solera for the TEM, SEM and Raman characterization, respectively. This work has been supported by the thematic network "Nanostructure advanced materials and applications in Mexico" between Spain and Mexico sponsoring this international collaboration. This work has been financially supported by Comunidad de Madrid, Spain (S2018/NMT-4411) and Ministry of Economia, Industría y Competividad (PID2019-106631GB-C43).

References

[1] S. Iijima, Helical microtubules of graphitic carbon, Nature 354 (1991) 56–58.
[2] B.C.Yadav Utkarsh Kumar, Synthesis of carbon nanotubes by direct liquid injection chemical vapor deposition method and its relevance for developing an ultra-sensitive room temperature based CO2 sensor, J. Taiwan Inst. Chem. Eng. 96 (2019) 652–663, https://doi.org/10.1016/j.jtice.2019.01.002.
[3] Hu Xiangang, Pengxiang Hou, Chang Liu, Huiming Cheng, Carbon nanotube/silicon heterojunctions for photovoltaic applications, Nano Mater. Sci. 1 (2019) 156–172, https://doi.org/10.1016/j.nanoms.2019.03.001.
[4] Fabricio N. Molinari, Edwin Barragán, Emanuel Bilbao, Luciano Patrone, Gustavo Giménez, Anahí V. Medrano, Alfredo Tolley, N. Monsalve Leandro, An

electrospun polymer composite with fullerene-multiwalled carbon nanotube exohedral complexes can act as memory device, Polymer 194 (2020), 122380, https://doi.org/10.1016/j.polymer.2020.122380.
[5] Guanyin Cheng, Xu Haitao, Ningfei Gao, Mengqin Zhang, Hailin Gao, Bihao Sun, Gu Mingxin, Yu Leyong, Yuanchang Lin, Xueqin Liu, Guotian He, Dapeng Wei, Carbon nanotubes field-effect transistor pressure sensor based on three-dimensional conformal force-sensitive gate modulation, Carbon 204 (2023) 456 464, https://doi.org/10.1016/j.carbon.2022.12.090.
[6] Xiaoqian Li, Xin Wang, Jie Deng, Min Li, Shuangshuang Shao, Jianwen Zhao, Printed carbon nanotube thin film transistors based on perhydropolysilazane-derived dielectrics for low power flexible electronics, Carbon 191 (2022) 267 276, https://doi.org/10.1016/j.carbon.2022.01.058.
[7] Manpreet Kaur Twinkle, Parveen Kumar Anjali, Bhanu Prakash, J.K. Gowsamy, Suresh Kumar, Multi-walled carbon nanotubes derived graphene nanoribbons for high performance supercapacitor applications, Mater. Chem. Phys. 296 (2023) 127204, https://doi.org/10.1016/j.matchemphys.2022.127204.
[8] C.H. Lui, Z. Ye, C. Keiser, X. Xiao, R. He, Temperature-activated layer-breathing vibrations in few-layer graphene, Nano Lett. 14 (2014) 4615 4621.
[9] Alamry Ali, Seyed Saeid Rahimian Koloor, Abdullah H. Alshehri, A. Arockiarajan, Carbon nanotube characteristics and enhancement effects on the mechanical features of polymerbased materials and structures A review, J. Mater. Res. Technol. 24 (2023) 6495 6521.
[10] C.C. Bowland, Y. Wang, A.K. Naskar, In: Development of nanoparticle embedded sizing for enhanced structural health monitoring of carbon fiber composites. Nondestructive characterization and monitoring of advanced materials, aerospace, and Civil infrastructure 2017. SPIE, 2017.
[11] N.N. Neha Arora, Sharma arc discharge synthesis of carbon nanotubes: comprehensive review, Diam. Relat. Mater. 50 (2014) 135 150, https://doi.org/10.1016/j.diamond.2014.10.001.
[12] Kazunori Anazawa, Kei Shimotani, Chikara Manabe, Hiroyuki Watanabe, Masaaki Shimizu, High-purity carbon nanotubes synthesis method by an arc discharging in magnetic field, Appl. Phys. Lett. 81 (2002) 739.
[13] Ayman M. Mostafa, Eman A. Mwafy, Nasser S. Awwad, A. Hala, Ibrahium Synthesis of multi-walled carbon nanotubes decorated with silver metallic nanoparticles as a catalytic degradable material via pulsed laser ablation in liquid media, Colloids Surf. A Physicochem. Eng. Asp. 626 (2021), 126992.
[14] Peiyu Ji, Jiali Chen, Tianyuan Huang, Lanjian Zhuge, Xuemei Wu, Hydrogen-modulated Ar/CH4 HWP-CVD for fast preparation of multi-wall carbon nanotube arrays with high specific capacitance, Diam. Relat. Mater. 109 (2020) 108067, https://doi.org/10.1016/j.diamond.2020.108067.
[15] Hong-Yan Lin, Jian Luan, Yuan Tian, Qian-Qian Liu, Xiu-Li Wang Thiophene-based Ni-coordination polymer as a catalyst precursor and promoter for multi-walled carbon nanotubes synthesis in CVD, J. Solid State Chem. 293 (2021), 121782, https://doi.org/10.1016/j.jssc.2020.121782.
[16] Emilio Muñoz-Sandoval, Alejandro J. Cortes-López, Beatriz Flores-Gómez, Juan L. Fajardo-Díaz, Roque Sánchez-Salas, Florentino López-Urías, Carbon sponge-type nanostructures based on coaxial nitrogen-doped multiwalled carbon nanotubes grown by CVD using benzylamine as precursor, Carbon 115 (2017) 409 421.
[17] Marcos Felisberto, Lazaros Tzounis, Leandro Sacco, Manfred Stamm, Roberto Candal, Gerardo H. Rubiolo, Silvia Goyanes, Carbon nanotubes grown on carbon fiber yarns by a low temperature CVD method: a significant enhancement of the interfacial adhesion between carbon fiber/epoxy matrix hierarchical composites, Comput. Commun. 3 (2017) 33 37.
[18] G. Pilatos, M. Samouhos, P. Angelopoulos, M. Taxiarchou, Ch. Veziri, R. Hutcheon, P. Tsakiridis, A.G. Kontos, Carbon nanotubes growth on expanded perlite particles via CVD method: the influence of the substrate morphology, Chem. Eng. J. 291 (2016) 106 114.
[19] Wu Yu-Tsung, Su Huan-Chieh, Chung-Min Tsai, Kuo-Liang Liu, Guo-Dung Chen, Ren-Hong Huang, Tri-Rung Yew, Carbon nanotube formation by laser direct writing, Appl. Phys. Lett. 93 (2008), 023108.
[20] B. Annubhawi Annu, Pramod K. Bhattacharya, P.K. Shukla Singh, Hee-Woo Rhee, Carbon nanotube using spray pyrolysis: recent scenario, J. Alloys Compd. 691 (15) (2017) 970 982.
[21] G. Kiruthiga, K.S. Rajni, N. Geethanjali, T. Raguram, E. Nandhakumar, N. Senthilkumar, SnO2: investigation of optical, structural, and electrical properties of transparent conductive oxide thin films prepared by nebulized spray pyrolysis for photovoltaic applications, Inorg. Chem. Commun. 145 (2022), 109968, https://doi.org/10.1016/j.inoche.2022.109968.
[22] Dae Soo Jung, Hye Young Koo, Sung Eun Wang, Seung Bin Park, Yun Chan Kang, Ultrasonic spray pyrolysis for air-stable copper particles and their conductive films, Acta Mater. 206 (2021), 116569, https://doi.org/10.1016/j.actamat.2020.116569.
[23] R.A. Afre, T. Soga, T. Jimbo, M. Kumar, Y. Ando, M. Sharon, Growth of vertically aligned carbon nanotubes on silicon and quartz substrate by spray pyrolysis of a natural precursor: turpentine oil, Chem. Phys. Lett. 414 (2005) 6 10.
[24] Nitin Dwivedi, Divyanshi Srivastava, Rajesh Kumar Shukla, Anchal Srivastava Spectroscopic Study of Large-Scale Synthesized, Nitrogen-doped carbon Nanotubes using Spray Pyrolysis Technique Materials Today: Proceedings 12, 2019, pp. 590 595, https://doi.org/10.1016/j.matpr.2019.03.102.
[25] Oh. Sion, Kyungmin Im, Jinsoo Kim, Spray pyrolysis facilitated construction of carbon nanotube-embedded hollow CoFe electrocatalysts demonstrating excellent durability and activity for the oxygen reduction reaction, J. Alloys Compd. 944 (2023), 169232, https://doi.org/10.1016/j.jallcom.2023.169232.
[26] R. Kamalakaran, M. Terrones, T. Seeger, Ph. Kohler-Redlich, M. Rühle, Y.A. Kim, T. Hayashi, M. Endo, Synthesis of thick and crystalline nanotube arrays by spray pyrolysis, Appl. Phys. Lett. 77 (2000) 3385 3387.
[27] Annubhawi Annu, B. Bhattacharya, Pramod K. Singh, P.K. Shukla, Hee-Woo Rhee, Carbon nanotube using spray pyrolysis: recent scenario, J. Alloys Compd. 691 (2017) 970 982, https://doi.org/10.1016/j.jallcom.2016.08.246.
[28] B. Zou, X.X. Wang, X.X. Huang, J.N. Wang, Continuous synthesis of graphene sheets by spray pyrolysis and their uses as catalysts for fuel cells, Chem. Commun. 51 (2015) 741 744.
[29] G. Pilatos, E.C. Vermisoglou, A. Perdikaki, E. Devlin, G.S. Pappas, G.E. Romanos, Nikos Boukos, Tatiana Giannakopoulou, Christos Trapalis, Nick K. Kanellopoulos, Georgios N. Karanikolos, One-step, in situ growth of unmodified graphene magnetic nanostructured composites, Carbon 66 (2014) 467 475.
[30] D. Graf, F. Molitor, K. Ensslin, C. Stampfer, A. Jungen, C. Hierold, L. Wirtz, Spatially resolved Raman spectroscopy of single- and few-layer graphene, Nano Lett. 7 (2007) 238 242.
[31] Y. Hao, Y. Wang, L. Wang, Z. Ni, Z. Wang, R. Wang, C. Keong Koo, Z. Shen, John T. L. Thong, Probing layer number and stacking order of few-layer graphene by Raman spectroscopy, Small 6 (2010) 195 200.
[32] M.A. Pimenta, G. Dresselhaus, M.S. Dresselhaus, L.G. Cancado, A. Jorio, R. Saito, Studying disorder in graphite-based systems by Raman spectroscopy, Phys. Chem. Chem. Phys. 9 (2007) 1276 1290.
[33] A.M. Rao, A. Jorio, M.A. Pimenta, M.S.S. Dantas, R. Saito, G. Dresselhaus, M. S. Dresselhaus, Polarized Raman study of aligned multiwalled carbon nanotubes, Phys. Rev. Lett. 84 (2000) 1820.
[34] G. Pilatos, A.V. Perdikaki, A. Sapalidis, G.S. Pappas, T. Giannakopoulou, D. Tsoutsou, E. Xenogiannopoulou, N. Boukos, A. Dimoulas, C. Trapalis, N. K. Kanellopoulos, Georgios N. Karanikolos, Graphene by one-step chemical vapor deposition from ferrocene vapors: properties and electrochemical evaluation, J. Appl. Phys. 119 (2016) 064303 064310.
[35] M. Zhou, J. Tang, Q. Cheng, G. Xu, P. Cui, L.C. Qin, Few-layer graphene obtained by electrochemical exfoliation of graphite cathode, Chem. Phys. Lett. 572 (2013) 61 65.
[36] H. Medina, Y.C. Lin, C. Jin, C.C. Lu, C.H. Yeh, K.P. Huang, K. Suenaga, J. Robertson, Po-Wen Chiu, Metal-free growth of nanographene on silicon oxides for transparent conducting applications, Adv. Funct. Mater. 22 (2012) 2123 2128.
[37] C. Shan, H. Tang, T. Wong, L. He, S.T. Lee, Facile synthesis of a large quantity of graphene by chemical vapor deposition: an advanced catalyst carrier, Adv. Mater. 24 (2012) 2491 2495.
[38] P. Tan, S. Zhang, K.T. Yue, F. Huang, Comparative Raman study of carbon nanotubes prepared by DC arc discharge and catalytic methods, J. Raman Spectrosc. 28 (1997) 369 372.
[39] Périne Landois, Mathieu Pinault, Mickaël Huard, Valérie Reita, Stéphan Rouzière, Pascale Launois, Martine Mayne-L Hermite, Nedjma Bendi, Structure in nascent carbon nanotubes revealed by spatially resolved Raman spectroscopy, Thin Solid Films 568 (2014) 102 110.
[40] Liliane Bokobza, Jean-Luc Bruneel, Michel Couzi, Raman spectroscopy as a tool for the analysis of carbon-based materials (highly oriented pyrolitic graphite, multilayer graphene and multi-wall carbon nanotubes) and of some of their elastomeric composites, Vib. Spectrosc. 74 (2014) 57 63.
[41] Aleksandra Wese ucha-Birczyńska, Aneta Frączek-Szczypta, Elżbieta D ugoń, Karolina Paciorek, Agata Bajowska, Aneta Kościelna, Marta B ażewicz, Application of Raman spectroscopy to study of the polymer foams modified in the volume and on the surface by carbon nanotubes, Vib. Spectrosc. 72 (2014) 50 56.
[42] G. Vitali, M. Rossi, M.L. Terranova, V. Sessa, Laser-induced structural modifications of glassy carbon surfaces, J. Appl. Phys. 77 (1995) 4307.
[43] Z.J. Zhang, B.Q. Wei, G. Ramnath, P.M. Ajayan, Substrate-site selective growth of aligned carbon nanotubes, Appl. Phys. Lett. 77 (2000) 3764 3766.
[44] C. Chen, Y. Zhang, Nanowelded Carbon Nanotubes. Nanoscience and Technology, Chapter 2, Springer-Verlag Berlin Heidelberg, 2009.
[45] S.B. Sinnot, R. Andrews, D. Qian, A.M. Rao, Z. Mao, E.C. Dickey, F. Derbyshire, Chem. Phys. Lett. 315 (1999) 25.
[46] R. Andrews, D. Jacques, A.M. Rao, F. Derbyshirea, D. Qian, X. Fan, E.C. Dickey, J. Chen, Continuous production of aligned carbon nanotubes: a step closer to commercial realization, Chem. Phys. Lett. 303 (1999) 467.
[47] E.R. Edwards, E.F. Antunes, E.C. Botelho, M.R. Baldan, E.J., Corat evaluation of residual iron in carbon nanotubes purified by acid treatments, Appl. Surf. Sci. 258 (2011) 641 648.
[48] Raji Atchudan, Arumugam Pandurangan, Jin Joo, Effects of nanofillers on the thermo-mechanical properties and chemical resistivity of epoxy nanocomposites, J. Nanosci. Nanotechnol. 15 (2015) 4255 4267.